ELSEVIER

Polymer 41 (2000) 1937–1946

polymer

Interface–property relationships in biaxially stretched PP–PET blends

J.-C. Lepers[a], B.D. Favis[a,*], S.L. Kent[b]

[a]*Centre de recherche appliquée sur les polymères, Department of Chemical Engineering, Ecole Polytechnique de Montréal, PO Box 6079 Stn "Centre-ville" Montreal, Quebec, Canada H3C3A7*

[b]*3M COMPANY, 3M Film Technology Center, 3M Center, BLDG236-GB-05, St. Paul, MN 55144-1000, USA*

Received 9 July 1998; received in revised form 25 April 1999; accepted 5 May 1999

Abstract

In this paper, the influence of the addition of a copolymer on the interface, molecular orientation and properties of biaxially stretched PP–PET is studied. For most homopolymers, biaxial stretching results in an improvement of the properties caused by chain orientation. Blending with a second homopolymer and creation of a multiphase system leads to the occurrence of decohesion phenomena between both polymers, the net result of which are diminished properties. In this work the decohesion process and the influence of an interfacial modifier on that phenomenon is measured quantitatively. In order to determine the point of interfacial saturation by the modifier, the morphology is also studied via the emulsification curve for this system. The crystallinity of the system is examined by WAXS. In most non-stretched polymer blends, it is the elongation at break and impact properties, which are the most significantly affected by the state of the interface. The process of biaxial stretching and resulting decohesion causes even a low strain property such as the Young's modulus to also become highly sensitive to the state of the interface. When a copolymer is added to the blend, the modulus and stress at break after stretching are dramatically improved compared with the uncompatibilized blend. It is shown for the 10%PP–90%PET blend, where decohesion was entirely suppressed by addition of the interfacial modifier, that maximum property improvement occurs at copolymer levels below interfacial saturation. WAXS measurements on the uncompatibilized biaxially stretched system demonstrate an isotropic system with respect to molecular orientation. Upon addition of the interfacial modifier preferential chain orientation is observed in the machine and transverse direction. This is related to the suppression of decohesion around the dispersed phase caused by the increased adhesion between the matrix and the dispersed phase.

Keywords: Polymer; Blends; Biaxial stretching

1. Introduction

For many years, companies producing plastic films have shown great interest in improving and controlling the mechanical properties of biaxially stretched films [1]. In addition, an increased use of blends of poly(ethylene terephthalate) (PET) is taking place in the food industry where films are required with barrier properties. Typically, commercial PET films are produced by processes involving either sequential or simultaneous biaxial stretching [2,3]. The simultaneous stretching is able to produce, in one step, an isotropic plane film and properties of such films have been extensively studied [4–7]. However, because of engineering problems associated with the production of these kind of films, sequential biaxial drawing remains the technique most often used to produce PET films.

Sequential biaxial stretching is in fact a uniaxial stretching in the "machine direction" (MD) followed by a second stretching in the "transverse direction". The deformation and the orientation occurring in PET films during stretching, and their effects on the properties were studied in detail by Gohil et al. [2,3,8,9] who showed by wide angle X-ray scattering (WAXS) that biaxial stretching induces crystallization and orientation of these crystals. During stretching, strain-induced crystalline structures appear. These crystals are believed to be small and possess defects. In the first step (MD stretching), the chain alignment is essentially in the MD direction, but this chain alignment decreases as the TD draw ratio increases. Crystalline texture development shifts from a fiber-like structure to a biaxial structure during the second step of stretching. On the other hand, a crystalline amorphous periodicity appears during stretching. During the first step (MD stretch), this periodicity is predominantly along the MD but will shift to the TD direction with the second step of stretching.

The stress–deformation relationship for stretched PET

* Corresponding author. Tel.: +1-514-340-4711; fax: +1-514-340-4159.
E-mail address: favis@chimie.polymtl.ca (B.D. Favis)

0032-3861/00/$ - see front matter
PII: S0032-3861(99)00341-9

films was studied in more detail by Gordon et al. [10] and by Buckley et al. [11,12] To explain the behavior of the PET films during uniaxial stretching, Gordon et al. [10] compared the optical properties (linked to the orientation) of their samples with the drawing stress and shrinkage stress (during relaxation) of uniaxially stretched PET samples. They showed that PET behaves, under stretching, like a molecular network which possesses an entanglement density of about 2×10^{26} m^{-3} which corresponds to between 14 and 21 monomer units per chain between entanglements. Buckley et al. [11,12] also studied the behavior of a PET during biaxial stretching, They modeled it with a three-dimensional glass–rubber constitutive model. The hot drawing of amorphous PET close to the T_g consists of a flow process constrained by the elasticity of a rubber-like network. Their model is based on the fact that the free energy consists of two additive components. One is due to local intra- and inter-molecular interactions, and relaxes in shear on an experimental time-scale; the other is due to the entropy of conformation of the chain molecules. They are able to predict the shape of the stress–strain relationship which showed an increase of the stress when the strain is increased, followed by a rubbery plateau and finally by a re-increase of the stress (strain hardening).

The above studies were carried out on pure PET, but a few authors [1,2,13,14] have also shown the effect of stretching and orientation on the properties of PET films blended with other polymers. Sambaru and Jabarin [13] studied the blend of PET–high density polyethylene (HDPE) compatibilized by a maleic anhydride grafted olefin. They showed that blends with compatibilizer displayed strain hardening upon stretching as described by Buckley, contrary to the non-compatibilized blend. They also observed that mechanical properties, such as the modulus and ultimate stress, showed an improvement upon orientation. All their studies were done at high compatibilizer concentration in order to attain saturation of the interface by the compatibilizer.

More recently, Gopalakrishnan et al. [14] studied the effect of a maleic anhydride grafted styrene–ethylene–butylene–styrene (SEBS-g-MA) on the permeability of a blend of PET–poly(ethylene-co-vinyl alcohol) (EVOH). They concluded that the impermeability was improved by the EVOH which passes from a spherical shape to a discus shape because of the stretching, increasing the path length for the gases diffusing through the polymer. Nevertheless, they did not see any effect of the compatibilizer. This is in contradiction with Carté et al. [15] who observed a significant improvement of the properties of a PET–PE blend compatibilized by the same copolymer.

In this study, the effect of a SEBS-g-MA interfacial modifier on the interface, molecular orientation and properties of a biaxially stretched PET–polypropylene (PP) blend is studied. The objective is to establish a relationship between the state of the interface and the mechanical properties of these blends. The state of the interface is evaluated using two techniques: the emulsification curve and apparent density measurements. The effect of interfacial modification on chain orientation is estimated by WAXS.

2. Experimental

2.1. Materials

The blends investigated in this study used PET as the matrix and PP as the dispersed phase. The PET resin was supplied by the Minnesota Mining and Manufacturing Company (3M): grade ER 651000 with a molecular weight (M_w) of 36 300 g/mol. The polypropylene sample was an isotactic polymer produced by Ziegler–Natta synthesis. Its molecular weight is: $M_n = 90\,000$ g/mol and $M_w = 391\,000$ g/mol. The antioxidant used was Irganox B-225 from Ciba-Geigy. The compatibilizer, a saturated styrene–ethylene–butylene–styrene (S–EB–S) triblock copolymer grafted with 2% maleic anhydride, was supplied by Shell under the name of Kraton FG1901. Its molecular weight is $M_n = M_w = 50\,000$ g/mol. The copolymer contained 30% styrene. Various concentrations of compatibilizer were used, from 0 wt.% to 17.5 wt.% SEBS-g-MA based on the weight of dispersed phase (PP). This copolymer has been shown to be an effective compatibilizer for this system in other studies from this laboratory [16].

2.2. Blend preparation

In order to blend the matrix, minor phase and compatibilizer, the extrusion was done in two steps. Prior to extrusion of the minor phase, the PP was dry blended with 0.02% of antioxidant to avoid any thermal degradation. The PP was then blended with the SEBS-g-MA in a 25 mm co-rotating twin screw extruder with $L/D = 50$. The temperature profile in the extruder was the following: 25–175–180–185–190–195–200–200–200–200–220°C. The amount of SEBS-g-MA was varied from 2.5 to 15% based on the weight of PP. The extruded PP/SEBS blends were pelletized at the exit.

The PET was dried for 12 h at 120°C to avoid degradation during the extrusion. It was then blended with the PP, with and without the SEBS-g-MA, in a 25 mm co-rotating twin screw extruder. The temperature profile was the following: 25–250–265–270–270–270–270–270–270–270–270°C. A neck tube joined the end of the extruder with the die used to obtain cast webs. The polymer exited at 9.1 kg/h and flowed onto a rotating cooled cylinder. Cast webs of about 600 μm of thickness and 28.5 cm of width were produced.. The extruder was purged for 5–7 min between blends. Samples were collected over a 10–15 min period. A total of 45 different compositions were prepared.

2.3. Biaxial stretching

Before stretching, the samples were cut into squares of 9×9 cm^2 and dried for 36 h in a desiccator at room

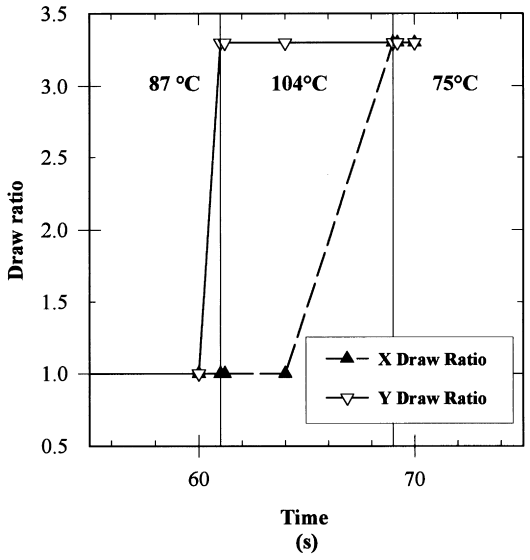

Fig. 1. Dependence of the temperature and of the *X* and *Y* draw ratio with time during the biaxial stretching.

temperature. Each sample was stretched in a T.M. Long laboratory stretcher. The evolution of the *X* and *Y* ratios and the temperature versus time are shown in Fig. 1. In this profile, *Y* direction stretching is done at a rate of 200%/s and a true stretch ratio of three followed by *X* direction stretching at a rate of 40%/s and a true stretch ratio of three. After stretching, the samples were quenched with air to avoid relaxation.

2.4. Morphological and image analysis of non-stretched films

Prior to observation, samples were microtomed at room temperature in the extrusion direction with a Leica Jung RM 2065 microtome equipped with a glass knife. The samples were then etched by immersion in trichlorobenzene at 140°C during 4 h to remove the minor phase (PP). Finally, the samples were covered by a gold–palladium alloy. A scanning electron microscope (Jeol model 820) was used to examine the shape and the size of the dispersed phase.

The semi-automatic image analyzer used to measure the diameters of the dispersed phase was developed in-house. The operation of this instrument has been described elsewhere [17]. Six SEM photomicrographs were analyzed for each sample to calculate the number average diameter, d_n, the volume average diameter, d_v, and the polydispersity (d_v/d_n), P_d, of the blends after twin screw extrusion. A correction factor [18] was applied to the diameters determined from SEM micrographs of microtome surfaces. On average, 200–300 diameter measurements were taken per blend preparation.

2.5. Mechanical measurements

The mechanical measurements were carried out on samples in both extrusion directions for the unstretched samples and both stretch directions for the biaxially stretched samples to examine if there were differences in orientation.

Measurements were carried out according to ASTM D 638 and D 682. Non-stretched samples were cut in the shape of type II dogbones as described in the standard. Stretched samples were cut into rectangles of $2.5 \times 12.5\ cm^2$. The standard recommends 10 cm between the grippers, but in our case, the value was decreased to 7.5 cm to be sure that all the zone stretched during the tensile test was uniformly biaxially stretched. Tests were carried out on samples containing 10 and 20% dispersed phase; the dispersed phase contained 0, 1.2, 3.75, and 10% SEBS-g-MA.

As recommended by the ASTM standards, unstretched samples were tested with a stretch speed of 10 mm/min and the stretched samples were tested with a speed of 50 mm/min. For each sample, the Young's modulus and stress at break were recorded. These different values are shown in Table 1 for the unstretched samples and in Table 2 for the stretched samples.

2.6. Density measurement

In order to measure the density of the samples, discs were cut with a punch, weighed and measured. The density of the samples after stretching is an indication of the adhesion in the material. When no cohesion exists at the interface during the stretching, voids will appear. These voids will increase the apparent volume of the sample and so decrease the density. The percentage of air present in the samples is obtained by comparing the density before and after stretching.

Table 1
Mechanical properties of PET, PP, PP–PET–SEBS unstretched blends

Young's modulus (MPa)								
PP–PET	0% SEBS	1.2% SEBS	3.75% SEBS	10% SEBS	10% SEBS (Kerner)	PP	PP–SEBS 10%	PET
20:80	1750	1660	1555	1470	1406	1000	1880	1880
10:90	1740	1640	1790	1670	1608			
Stress at break (MPa)								
PP–PET	0% SEBS	1.2% SEBS	3.75% SEBS	10% SEBS	PP	PET		
20:80	32	36	40	37	35	50		
10:90	41	44	44	44				

Table 2
Mechanical properties of PET and PP–PET–SEBS stretched blends (for each composition the value on the left corresponds to the machine direction samples and the value on the right to the transverse direction)

Young's modulus (MPa)										
PP–PET	0% SEBS		1.2% SEBS		3.75% SEBS		10% SEBS		PET	
20:80	780	1070	950	1170	2480	3410	2320	3020	3400	5260
10:90	1770	2090	2060	2750	2880	4330	2720	3750		
Stress at break (MPa)										
PP–PET	0% SEBS		1.2% SEBS		3.75% SEBS		10% SEBS		PET	
20:80	35.5	32.8	41.1	35.4	93.3	88.2	89.9	84.1	185.7	174.4
10:90	67.5	67.8	78.1	80.0	132.4	124.8	137.4	116.1		

2.7. WAXS measurement

The orientation observed in the sample was characterized by WAXS. These experiments were conducted in the transmission mode using nickel filtered CuKα radiation ($l = 1.54178$ Å) and a flat-film camera (Warhus). The X-ray beam was oriented directly perpendicular to the film. The sample-to-film distance was about 75 mm and is calibrated by an unstretched PET film. The typical exposure time was 36 h. Daubeny et al. [19] identified PET as having a triclinic cell structure with lattice constants: $a = 4.56$ Å, $b = 5.94$ Å, $c = 10.75$ Å, $\alpha = 98.5°$, $\beta = 118°$, $\gamma = 112°$. The monoclinic unit cell parameters $a = 6.67$ Å, $b = 20.84$ Å, $c = 6.495$ Å, $\beta = 99.33°$ were obtained by starting with the values given in the literature [20–22] for the α-form of isotactic-PP. The crystal reflections and their Bragg angles are given in Table 3 for both homopolymers.

3. Results and discussion

3.1. Unstretched blend

3.1.1. Emulsification

The dependence of the dispersed phase size diameter as a function of the percentage of compatibilizer is shown for unstretched samples in Fig. 2(a) and (b). It is important to point out that no significant skin-core effects and no orientation of the dispersed phase were observed in the cast web samples. The shape of the curves presented in Fig. 2 are typical of an emulsification curve [23–25]. The addition of the copolymer causes a reduction of the dispersed phase size until saturation of the interface is achieved. At that point, a leveling off of the dispersed phase size is observed. For all blends (10 and 20% dispersed phase), the initial diameter, diameter at saturation, critical concentration, and the interfacial area per molecule are given in Table 4.

Table 3
Experimental and calculated values (in degrees) of the Bragg angle (2θ) for different polyethylene terephthalate and isotactic polypropylene crystal reflections

Crystal reflections	2θ	
	Calculated	Experimental (±0.02)
PET		
− 1,1,1	21.31	21.39
0,1,0	17.53	17.49
0, − 1,1	16.41	16.22
PP		
1,3,0	18.57	18.39
0,4,0	17.02	16.81
1,1,0	13.96	14.11

From Fig. 2, it can be seen that the size of the dispersed phase is greater for the 20:80 blend than for the 10:90 blend. This is independent of the presence or absence of copolymer. In addition, the reduction of the dispersed phase size with copolymer is larger for the 10:90 blends. Rather than referring to a point of interfacial saturation, it is a better practice to refer to a region of interfacial modifier concentrations where interfacial saturation is achieved. By comparing the plateau values of both the d_v and d_n as determined via image analysis, it can be seen that the 10% system achieves interfacial saturation in the range of 3.7–5.0% interfacial modifier whereas the 20% system achieves interfacial saturation in a lower range between 2.5–3.7% interfacial modifier. In the latter case although equilibrium is achieved at 2.5% for the d_n, it is clear that at that same concentration the d_v has not quite achieved its plateau value. In order to understand the differences between the two emulsification curves, the interfacial area occupied per molecule of copolymer is calculated as described elsewere [23–25]. The interfacial area calculation is made assuming all the modifier is at the interface which is highly unlikely in this type of reactive blend system. These areas therefore represent a lower limiting value. The calculated interfacial areas occupied per molecule are given in Table 4 and are similar for both the 10:90 and the 20:80 blends. This indicates that the variation in the steady state particle size and critical concentration is not likely due to enhanced micelle formation. Micelle formation generally results in artificially lower values of interfacial area occupied per molecule as estimated from the emulsification curve [26].

The most probable reason explaining why the dispersed phase diameters are higher for the 20:80 blend is that a flat rectangular die was used after twin-screw extrusion. This renders the process highly coalescence sensitive. In the die, in the absence of mixing, the time allowed for coalescence is

Table 4
Morphological characteristics of the PP–PET blends

PP–PET	Initial d_v (μm)	Saturation d_v (μm)	Critical concentration (%)	Interfacial area per molecule (nm^2)
10:90	9.8	4.3	5	4.0
20:80	12.1	6.4	3.5	3.8

significantly increased. For that reason, the coalescence process is really at the boundary between a dynamic and a quasi-static phenomenon. It has recently been suggested that it is more difficult to prevent static coalescence [27]. In the 20:80 blend, the copolymer is not able to suppress all the coalescence even when saturation of the interface is achieved. The importance of coalescence is confirmed by a previous study of the PET–PP blend by Lepers et al. [16] who found that, in a shear mixer, the dispersed phase size is decreased by a factor of 3.4 times when copolymer is added. In that case, it was possible to prevent almost all the coalescence by the addition of the copolymer. Nevertheless, in that study, the morphology development was studied in a dynamic mixing environment. The severity of coalescence in the present case is further confirmed by plotting the evolution of the dispersed phase size as a function of the dispersed phase concentration (Fig. 3). This figure shows that the dispersed phase size increases significantly with concentration even when compatibilizer is present. In contrast, other studies carried out under dynamic conditions in a brabender mixer have shown that an interfacial modifier can suppress coalescence phenomena over a large composition range [26,28,29].

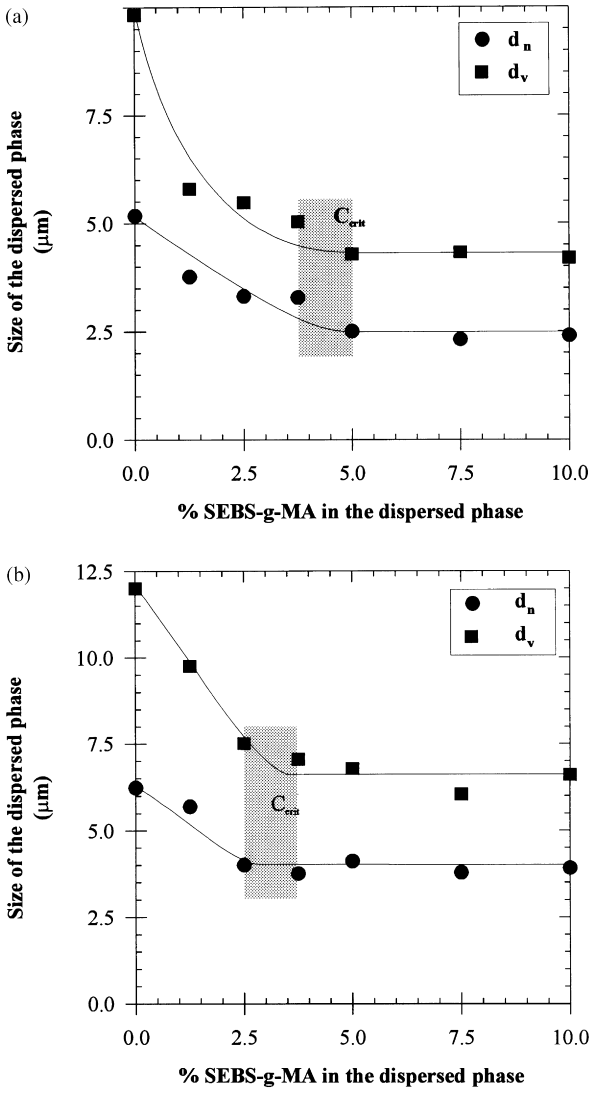

Fig. 2. Emulsification curves for the (a) 10:90 and (b) 20:80 PP–PET blends. The concentration region for interfacial saturation is shaded.

3.1.2. Void volume

The void volume for the unstretched blend system is essentially zero, indicating no significant level of decohesion exists around the dispersed phase particle.

3.1.3. Mechanical properties

Figs. 4 and 5 illustrate the evolution of the Young's modulus and of the stress at break for the 10:90 and 20:80 unstretched blends as a function of the percentage of copolymer in the blend. No significant differences in the tensile mechanical properties between the two directions (machine and transverse) were observed. This indicates that the extrusion did not cause orientation in the samples.

In Fig. 4, different tendencies may be observed. The addition of the PP in the matrix causes a decrease of the modulus due to the low modulus of the polypropylene compared with that of the PET. A sharp decrease of the modulus is observed with the addition of copolymer, essentially between 0 and

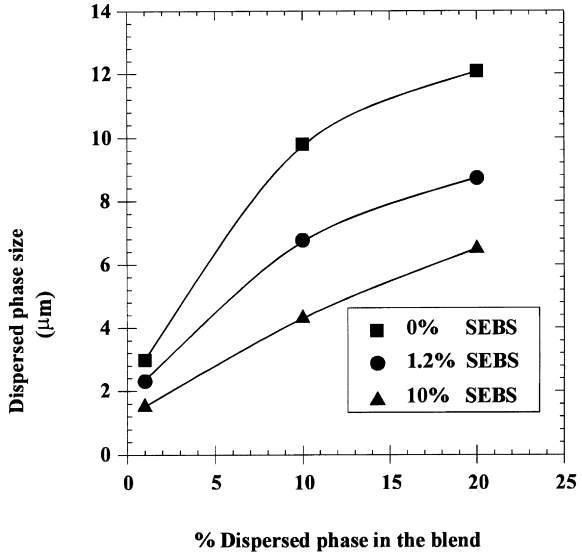

Fig. 3. Dependence of the dispersed phase size as a function of the dispersed phase concentration.

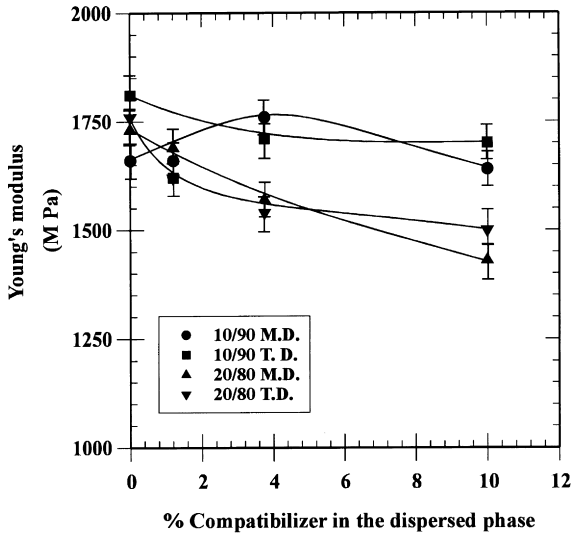

Fig. 4. Young's modulus as a function of the percentage copolymer in the dispersed phase for the 10:90 and 20:80 PP–PET unstretched blends in the machine and transverse direction.

3.75% of compatibilizer. This decrease is likely due to the elastomeric properties of this copolymer. In order to evaluate if there is adhesion between the matrix and the dispersed phase, the Kerner [30] model for perfect adhesion has been used to estimate the Young's modulus for the blends containing 10% copolymer. These values are given in Table 1. The similarity of the calculated and the experimental values indicate that in the case of these unstretched blends containing 10% copolymer, the matrix and the dispersed phase demonstrate a high level of adhesion.

3.2. Effect of biaxial stretching

3.2.1. Pure PET

Comparing Tables 1 and 2 shows that the mechanical properties of the pure PET are significantly improved after biaxial stretching, as expected. Moreover, the Young's moduli are higher in the transverse direction than in the machine direction. This is in agreement with the hypothesis that the orientation due to the stretching is more significant in the second direction of stretching (TD) [2,3,8,9]. In Fig. 6(a) WAXS measurements on pure PET confirm that a preferential orientation appears in the MD and TD direction as demonstrated by an increase in the intensity at the poles and the equator in the (0, − 1,1) reflection plane. However, since no annealing was carried out on the samples, the crystallinity is low and does not permit one to distinguish the difference between the MD and TD orientation as was done by Chang et al. [9]. As discussed in the introduction, the first step (MD stretching) creates a population of poorly formed crystallites which have their chain axis oriented preferentially along the MD. The TD draw disrupts the chain alignment in the MD, as well as shears and destroys partially strain-induced crystalline embryos, hence reforming a new local alignment in the TD as shown in the literature [2,3,8]. This alignment is responsible for the increased mechanical properties of the stretched PET (Table 2) as compared to the unstretched PET (Table 1).

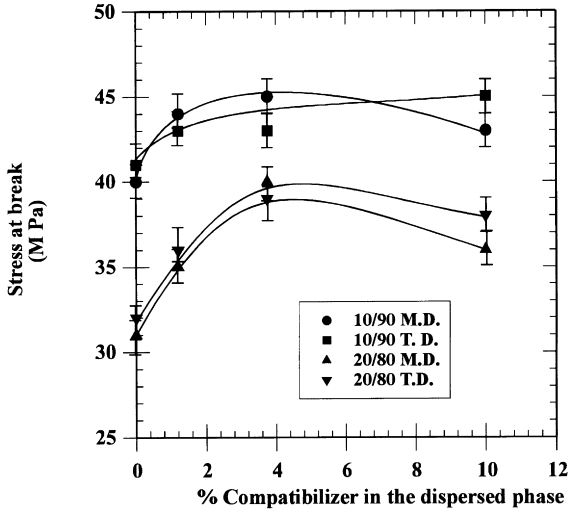

Fig. 5. Stress at break as a function of the percentage copolymer in the dispersed phase for the 10:90 and 20:80 PP–PET unstretched blends in the machine and transverse direction.

3.2.2. Binary PET–PP blends

The addition of a dispersed phase drastically changes the behavior of the biaxially stretched PET (Table 2). As observed for the unstretched samples, the presence of polypropylene results in a decrease of the tensile mechanical properties as compared to both pure PET and unstretched PET–PP (Table 2). Increasing the amount of dispersed phase from 10 to 20% results in large decreases in the modulus and the stress at break. This decrease in the mechanical properties is much greater than can be accounted for by the simple presence of PP.

The morphology of a PP–PET (20:80) blend observed by SEM perpendicular to the TD direction is presented in Fig. 7(a). The morphology clearly shows that pronounced decohesion occurs at the interface. Observations performed perpendicular to the MD direction and on blends containing 10% PP yield the same results. Due to the poor adhesion, voids form around the dispersed phase during stretching. By measuring the apparent density of the samples, the volume of air, which is contained in the voids, can be approximated. Fig. 8 presents the dependence of the void volume and of the dispersed phase interfacial area as a function of the concentration of dispersed PP phase for binary PP–PET blends. As shown in this figure, increasing the amount of dispersed phase results in a significant increase of the void volume fraction present in the samples. This is directly related to the higher dispersed phase interfacial area at higher compositions.

In order to understand what is occurring during the stretching with respect to chain orientation, film plane WAXS patterns of the stretched PP–PET (10:90) blend are presented in Fig. 6(b). A perfect ring is observed for

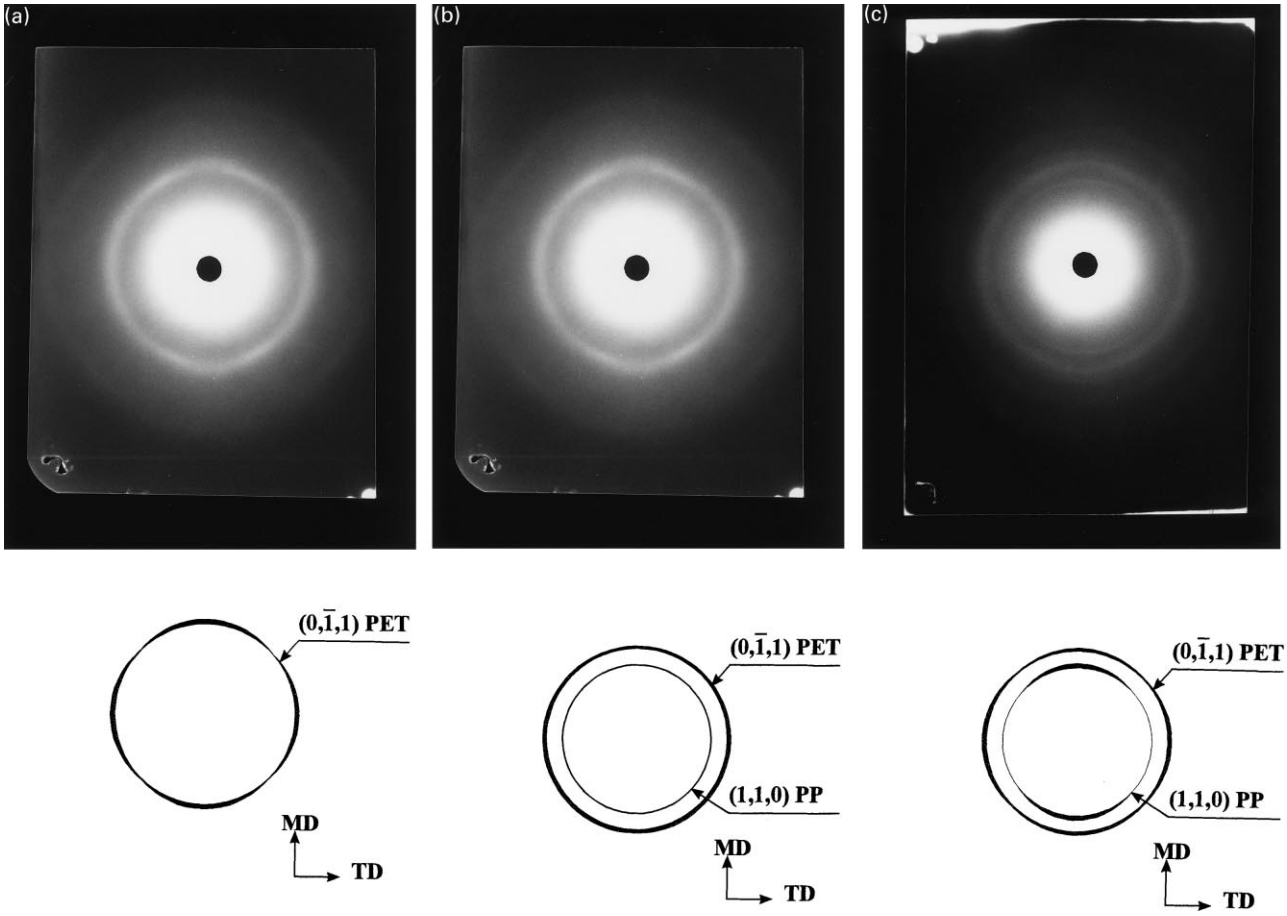

Fig. 6. Film plate WAXS patterns of the as-drawn sequential films. MD vertical and TD horizontal: (a) pure PET; (b) PP–PET (10:90) non-compatibilized; (c) PP–PET (10:90) with 10% SEBS-g-MA in the PP.

the (0, − 1,1) reflection plane of the PET and for the (1,1,0) reflection plane of the PP. This indicates that this material is highly isotropic. Some small orientation, however, likely remains in the TD direction as reflected in the mechanical properties. The same observations were made for the PP–PET (20:80) blend.

From the above results on the biaxially stretched binary PP–PET blends, it is clear that the decohesion occurring during the stretching due to the poor adhesion does not permit the PET chains to effectively orient. The significantly diminished properties after biaxial stretching of the binary blend as compared to pure PET are thus principally due to decohesion phenomena and reduced PET chain orientation. In effect the dispersed phase is air.

3.2.3. Compatibilized PET–PP blends

The dependence of the void volume as well as the modulus and stress at break as a function of the amount of copolymer in the minor phase are shown in Figs. 9–11 and in Table 2. In contrast with the results obtained for the unstretched blends, an increase in both modulus and stress at break is observed with copolymer concentration with values achieving a maximum value at particular levels of interfacial modifier. It appears that the 10%PP–PET blend attains maximum properties once 2.5% copolymer is added while the 20% PP–PET system attains its maximum values closer to levels of 4% of interfacial modifier. Moreover, the Young's moduli are higher in the transverse direction than in the machine direction as observed for the pure PET.

The morphology of the PET–PP (80:20) blend compatibilized with 10% SEBS-g-MA observed parallel to the MD direction is presented in Fig. 7(b) and (c). The dispersed phase is visible in the shape of elongated ellipsoids. Similar results were obtained for the 10% PP blend. No apparent decohesion was observed for any of these blends via SEM. A quantitative estimation of decohesion phenomena is presented for blends containing 10 and 20% as a function of copolymer concentration in Fig. 9. This figure shows clearly that the addition of the copolymer results in a decrease of the void volume appearing in the samples during stretching. It is interesting to note that the void volume is reduced to zero after addition of the interfacial modifier in the case of the 10:90 PP–PET blend, but that a low level of residual voiding remains in the 20% blend even after addition of significant levels of interfacial modifier. Further the minimum void volume is achieved at a level of 4% copolymer concentration for the 20:80 blend and at about 5% copolymer concentration for the 10:90 blend. Both these

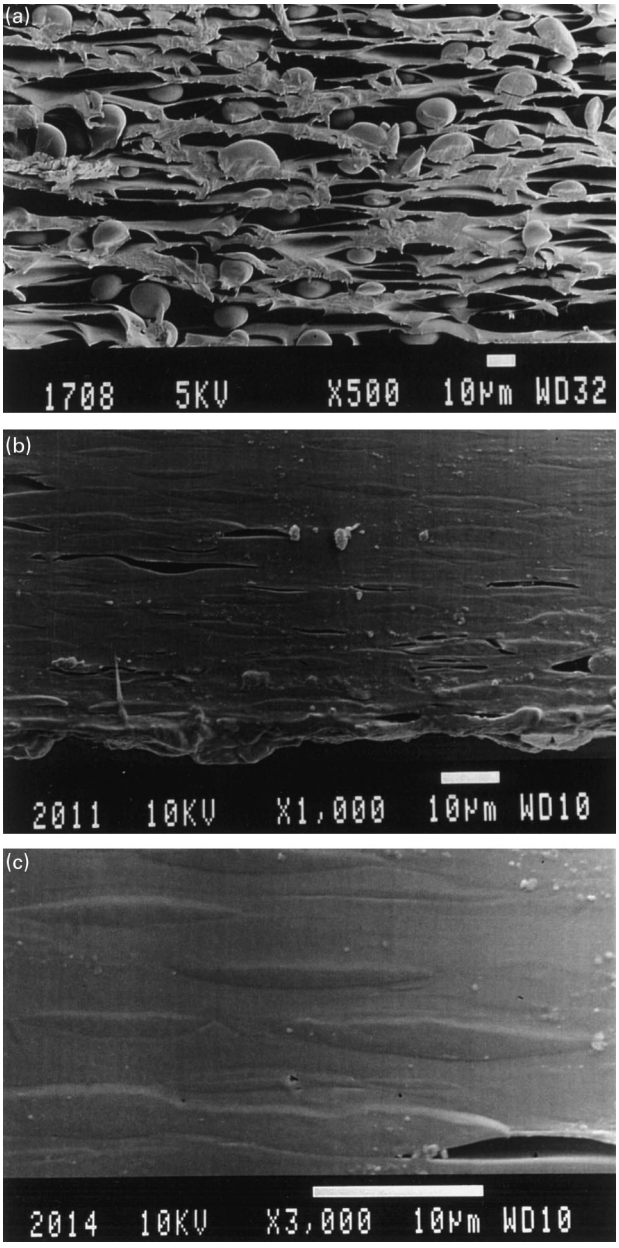

Fig. 7. Morpology of the stretched blends: (a) PP–PET (20:80) non-compatibilized, (b) and (c) PP–PET (20:80) with 10% SEBS-g-MA in the PP. (Scale bar represents 10 microns.)

values correspond closely to the critical concentration zones for interfacial saturation presented in the emulsification curve in Fig. 2. In fact the trends observed in the emulsification and void volume curves are very similar to one another. The non-zero void volume value for the 20:80 PP–PET blend is not likely due to a difference in the structure of the interface since, as mentioned previously, the area occupied per modifier molecule as calculated from the emulsification curve is identical in both cases. A possible explanation may be that the higher steady state dispersed phase size for the 20% compatibilized blend results in a somewhat higher concentration of stresses at the interface during stretching resulting in some low levels of voiding.

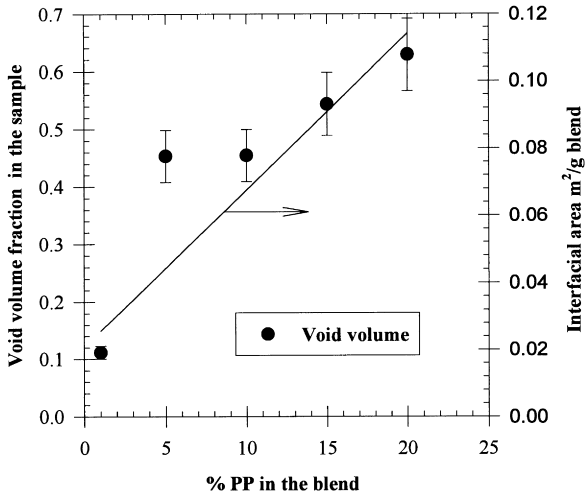

Fig. 8. Void volume as a function of the dispersed phase composition for the uncompatibilized biaxially stretched blend samples. The solid line demonstrates the interfacial area dependence.

In order to study the effect of the copolymer on the orientation, the film plane WAXS patterns of the stretched PET–PP (90:10) blend compatibilized with 10% SEBS is presented in Fig. 6(c). The (0, − 1,1) reflection plane of the PET is a ring having maximum intensity at the equator (TD direction) and at the poles (MD direction). This is an indication that the PET matrix has recovered a certain level of orientation compared with the uncompatibilized blend. Nevertheless, this orientation is less than that of the pure PET as demonstrated by both the mechanical properties and the WAXS patterns. In addition, the (1,1,0) reflection plane of the PP showed that the stretching has also induced an orientation of the dispersed phase. The orientation of the PP is pronounced in the MD direction because the first

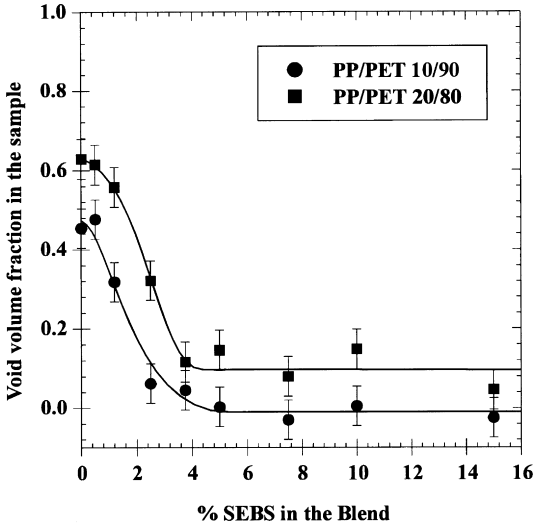

Fig. 9. Void volume as a function of the percentage interfacial modifier in the 10:90 and 20:80 biaxially stretched blend.

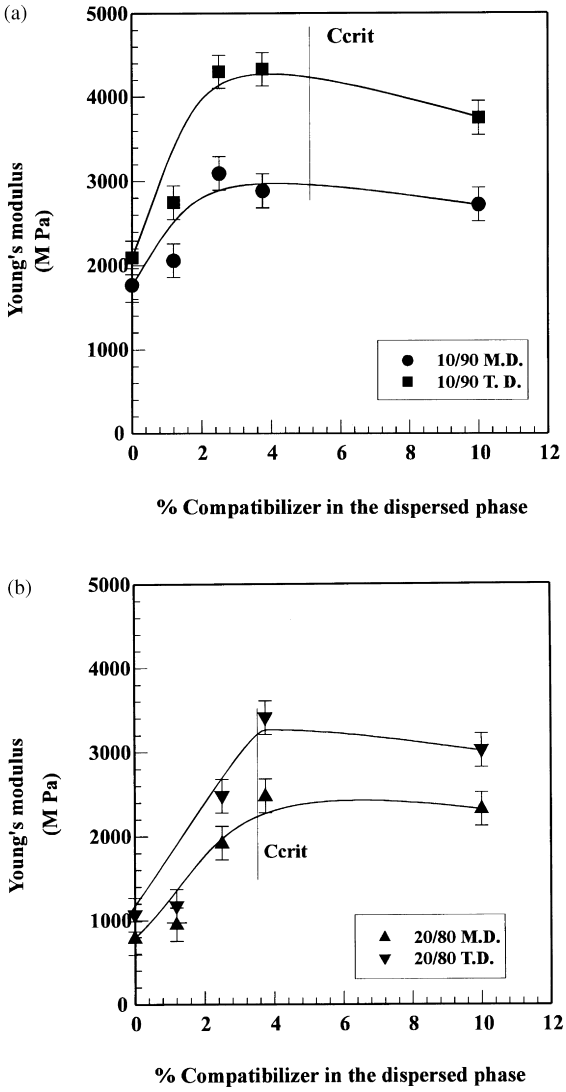

Fig. 10. Young's modulus as a function of the % copolymer in the dispersed phase in the machine and transverse direction for the (a) 10:90 and (b) 20:80 PP–PET stretched blends. The critical concentration for interfacial saturation from Fig. 2 is shown.

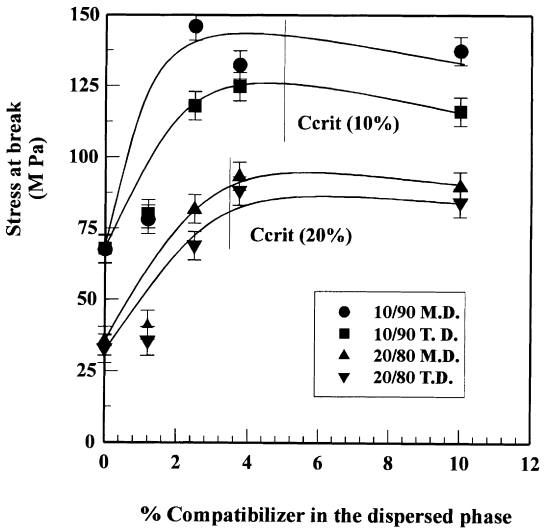

Fig. 11. Stress at break as a function of the percentage copolymer in the dispersed phase in the machine and transverse direction for the 10:90 and 20:80 PP–PET stretched blends. The critical concentration for interfacial saturation from Fig. 2 is shown.

stretching (MD) is carried out at lower temperature than the second (TD). The stretching of the PP is accomplished more easily than the stretching of the PET. This is due in part to their relative modulus (Table 1) and also because the stretching temperatures are within the same range as the glass transition temperature of the polyester (70°C/80°C), but are about 100°C higher than the glass transition temperature of the PP (−10°C/−20°C).

3.2.4. Relationship between the state of the interface and mechanical properties

Biaxial stretching of uncompatibilized blends renders the mechanical properties highly sensitive to the interface due to interfacial decohesion. In melt processed, unstretched blends, the properties most sensitive to the state of the interface are high strain properties such as impact strength and elongation at break. In the case of biaxial stretching, even a low deformation property, such as the Young's modulus, is drastically increased by the addition of an interfacial modifier.

Using the apparent density study combined with the emulsification curve, it is possible to evaluate the importance of both interfacial voiding and interfacial saturation on the mechanical properties. As mentioned before there is a close correspondence between the interfacial voiding dependence and the emulsification curve. From Figs. 10 and 11, it is interesting to note that the 10%PP–90%PET blend attains its maximum in Young's modulus and stress at break at values clearly below the critical concentration for saturation of the interface (Fig. 2). This indicates that once the level of decohesion has been significantly diminished, saturation of the interface is not a necessary requirement for improvement of those particular properties. In contrast, the 20% PP–80%PET blend attains its maximum in Young's modulus and stress at break at values of the modifier closely related to its critical concentration for saturation of the interface. As was mentioned earlier, despite the fact that the interface is saturated with copolymer, a residual void volume remains after biaxial stretching of the 20%PP–80%PET blend even at high levels of interfacial modifier (Fig. 9). Likely, in order to compensate for this effect, a higher level of interfacial modifier is required to achieve the maximum in mechanical properties for that system. In any case it is evident from the 10%PP–90%PET data that interfacial saturation is not a necessary requirement to arrive at values of maximum modulus and strain at break. This behavior is in contrast to previous impact strength studies [31–33] on melt processed unstretched blends where fragile to ductile transitions were found to be closely related to the

critical concentration of modifier required for interfacial saturation.

The mechanical properties of the 20% system systematically display lower values than the 10% blend. This difference is essentially related to two sources. Firstly, the presence of the PP in the blend causes a decrease of the modulus as shown for the unstretched blend. Secondly, at all levels of copolymer addition a higher level of interfacial voiding is observed for the 20% blend.

4. Conclusions

In this study, the effect of a SEBS-g-MA interfacial modifier on the interface, molecular orientation and properties of a biaxially stretched PP–PET blend has been studied. The state of the interface was characterized through the use of the emulsification curve, which yields the quantity of interfacial modifier necessary for interfacial saturation, as well as by apparent density measurements, which quantified the level of interfacial voiding. In this way relationships were established between the state of the interface, molecular orientation as measured by WAXS and the mechanical properties of these blends.

In the pure PET, the stretching yields an improvement of the properties by inducing an orientation of the polymer chains, as expected. The addition of an immiscible second polymer (PP) decreases this orientation and substantially diminishes the mechanical properties. The decrease in properties is attributed to both the reduced molecular orientation as well as the development of interfacial voids during the stretching. It is the development of voids during stretching which inhibit a preferential orientation of the polymer chains. When an interfacial modifier, SEBS-g-MA, is added to the blends, it improves the interfacial adhesion and decreases the void volume present in the blends. The lower limiting void volume value was achieved at a modifier concentration closely related to the saturation of the interface from the morphological emulsification curve. This reduction in voiding with the addition of modifier allows a certain level of orientation to be recovered, both of which increase the properties, compared with the uncompatibilized blend. It is shown for the case of the 10:90 PP–PET blend that the maximum plateau in modulus and stress at break as a function of interfacial modifier content are achieved at concentration values well below interfacial saturation. In unstretched blends, only high deformation properties such as elongation at break or impact properties are dramatically modified by the addition of a compatibilizer. In biaxially stretched systems, since the addition of the interfacial modifier results in decreased interfacial voiding as well as increased chain orientation, even low deformation properties such as the Young's modulus exhibit substantial improvements (three-fold increase in the case of the 20:80 PP–PET blend).

Acknowledgements

This work was made possible by financial support from the Minnesota Mining and Manufacturing Company (3M), St. Paul, Minnesota, and by the "Fonds pour la formation de chercheurs et l'aide à la recherche" (FCAR) through a scholarship to J.-C. Lepers. The authors acknowledge Drs. Ron Tabar and David. T. Okamoto of 3M, St. Paul, for fruitful discussions and assistance. The authors also acknowledge Professor François Brisse who provided the opportunity to perform the WAXS measurements in the Chemistry Department of the University of Montreal and Dr. Michel Simard for his availability, helpful discussions and assistance with the WAXS measurements.

References

[1] Faisant de Champchesnel JB, Bower DI, Ward IM, Tassin JF, Lorentz G. Polymer 1993;34:3763.
[2] Gohil RM. J Appl Polym Sci 1994;52:925.
[3] Gohil RM. J Appl Polym Sci 1993;48:1649.
[4] Petermann J, Rieck U. J Polym Sci: Polym Phys 1987;35:279.
[5] Peszkin PN, Schultz JM, Lin JS. J Polym Sci: Polym Phys 1986;24:2591.
[6] Gupta VB, Kumar S. J Appl Polym Sci 1981;26:1897.
[7] Huisman R, Heuvel HM. J Appl Polym Sci 1989;37:595.
[8] Gohil RM, Salem RH. J Appl Polym Sci 1993;47:1989.
[9] Chang H, Schultz JM, Gohil RM. J Macromol Sci—Phys B 1993;32:99.
[10] Gordon DH, Ducket RA, Ward IM. Polymer 1994;35:2555.
[11] Buckley CP, Salem DR. J Appl Polym Sci 1990;41:1707.
[12] Buckley CP, Salem DR. Polymer 1987;28:69.
[13] Sambaru P, Jabarin SA. Polym Engng Sci 1993;33:827.
[14] Gopalakrishnan R, Schultz JM, Gohil RM. J Appl Polym Sci 1995;56:1749.
[15] Carté TL, Moet A. J Appl Polym Sci 1993;48:611.
[16] Lepers J-C, Favis BD, Tabar RJ. J Polym Sci: Polym Phys 1997;35:2271.
[17] Favis BD, Chalifoux JP. Polym Engng Sci 1987;27:1591.
[18] Saltikov SA. Proc Second Int Congr for Stereology. New York: H. Elias, 1967.
[19] Dauberny RD, Bunn CW, Brawn CD. Proc Roy Soc 1954;226A:531.
[20] Burke PE, Weatherly GC, Woodhams RT. Polym Engng Sci 1987;27:518.
[21] Tate KR, Perrin AR, Woodhams RT. Polym Engng Sci 1988;28:1264.
[22] Krigbaum WR, Roe RJ. J Chem Phys 1964;41:737.
[23] Favis BD. Polymer 1994;35:1552.
[24] Matos M, Favis BD, Lomellini P. Polymer 1995;36:3899.
[25] Cigana P, Favis BD, Jérôme R. J Polym Sci: Polym Phys 1996;34:1691.
[26] Cigana P, Favis BD. Polymer 1998;39:3373.
[27] Macosko CW, Guégan P, Khandpur AK, Nakayama A, Marechal P, Inoue T. Macromolecules 1996;29:5590.
[28] Willis JM, Favis BD, Lunt J. Polym Engng Sci 1990;30:1073.
[29] Favis BD, Cigana P, Matos M, Tremblay A. Can J Chem Engng 1997;75:273.
[30] Kerner EH. Proc Phys Soc 1956;69B:808.
[31] Cigana P, Favis BD, Albert C, Vu-Khanh T. Macromolecules 1997;30:4163.
[32] Lacasse C, Favis BD. Adv Polym Technol 1999; in press.
[33] Polizu S, Favis BD, VuKhanh T. Macromolecules 1999;32:3448.